Journal of Molecular Structure 1093 (2015) 208–218

Contents lists available at ScienceDirect

Journal of Molecular Structure

journal homepage: www.elsevier.com/locate/molstruc

Trans-dichlorotetrakis(1*H*-pyrazole-κN^2)copper(II): Synthesis, crystal structure, hydrogen bonding graph-sets, vibrational and DFT studies

Amani Direm [a,b,*], Mahir Tursun [c], Cemal Parlak [c], Nourredine Benali-Cherif [a]

[a] Laboratoire des Structures, Propriétés et Interactions Interatomiques LASPI²A, Département des Sciences de la Matière, Faculté des Sciences et Technologie, Université "Abbes Laghrour", Khenchela 40.000, Algeria
[b] Département de Chimie, Faculté des Sciences Exactes, Université de Constantine 1, Constantine 25.000, Algeria
[c] Department of Physics, Dumlupinar University, Kütahya 43100, Turkey

HIGHLIGHTS

- *Trans*-dichlorotetrakis(1*H*-pyrazole-κN^2)copper(II) were synthesized and characterized.
- The complex crystallizes in the monoclinic system, space group C2/c.
- The C_i symmetry is more stable than the C_1 symmetry.
- Structure is held together through N—H···Cl hydrogen bonds.

GRAPHICAL ABSTRACT

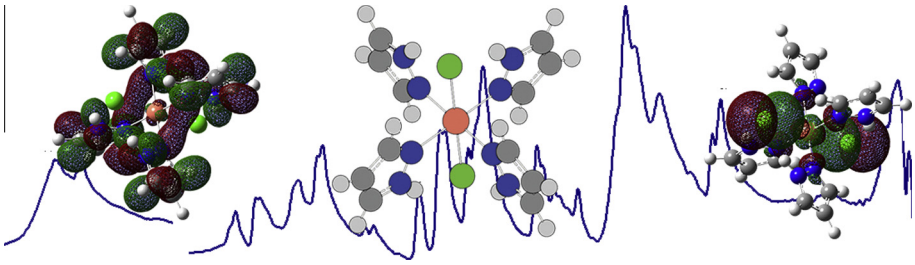

ARTICLE INFO

Article history:
Received 21 January 2015
Received in revised form 27 March 2015
Accepted 30 March 2015
Available online 3 April 2015

Keywords:
Pyrazole complexes
Crystal structure
Hydrogen-bonding
Vibrational spectra
DFT

ABSTRACT

The copper complex $[Cu(HPrz)_4]Cl_2$ (HPrz = Pyrazole) was synthesized and its structure was characterized by FT-IR, Raman and single-crystal X-ray diffraction (XRD) techniques. The structural conformers, optimized geometric parameters, normal mode frequencies and corresponding vibrational assignments of the compound were examined by means of the density functional theory (DFT) method, the Becke-3-Lee–Yang–Parr (B3LYP) functional, the 6-311+G(3df,p) and lanl2dz basis sets. Reliable vibrational assignments were investigated by the potential energy distribution (PED) analysis. The compound crystallizes in the monoclinic space group C2/c with the unit cell parameters $a = 13.5430$ (10) Å, $b = 9.1480$ (10) Å, $c = 14.6480$ (10) Å and $\beta = 116.7°$ (5). There is a good agreement between the theoretically predicted structural parameters and vibrational frequencies and those obtained experimentally. The findings of this work reveals further insight into molecular copper(II) pyrazole systems.

Introduction

Metal organic frameworks (MOFs) consist of metal ions or clusters often coordinated to rigid organic molecules to form one-, two-, or three-dimensional structures. MOFs are also known as coordination polymers which are the inorganic or organometallic polymer structures containing metal cation centers linked by organic ligands. The chemical and pharmacological properties of the pyrazoles have been investigated extensively, due to their chelating ability with metal ions [1] as terminal [2,3] or bridging ligands [4–6] and, precursors for synthesis of various multi-nitrogen donor ligands in the coordination, bio-inorganic and organometallic chemistry [7]. They are well known for the discovery of new catalyst precursors [8] and, for their potentially benefic chemical, biological and medicinal activities reported in the literature; including analgesic [9], anti-inflammatory [10] and other therapeutic functions. Furthermore, the pyrazoles are widely used for their ability to participate in hydrogen bonding interactions

* Corresponding author at: Laboratoire des Structures, Propriétés et Interactions Interatomiques LASPI²A, Département des Sciences de la Matière, Faculté des Sciences et Technologie, Université "Abbes Laghrour", Khenchela 40.000, Algeria. Tel.: +213 772 33 02 87.
E-mail address: amani_direm@yahoo.fr (A. Direm).

http://dx.doi.org/10.1016/j.molstruc.2015.03.068
0022-2860/

[11,12], as bridging units for two metal centers [13,14], and for the synthesis of complexes with spin crossover behavior [15].

The discrete complex *trans*-dichlorotetrakis(1*H*-pyrazole-κN^2)copper(II) had been mentioned in the earlier literature. In the early seventies, Reedijk [16] first published serial investigations about pyrazole and its derivatives. Mighell and coworkers also synthesized this complex and found the same unit cell [17]. It was synthesized by Sun and coworkers [18] in 2001, reacting hydrated copper chloride with a hydrotris(pyrazolyl)borate (Tp) derivative $[FeTp_2][TpFe(SCN)_3]$ in a methanolic solution. The UV–Vis and X-band ESR spectroscopic parameters of the complex were reported. Synthesis of $[Cu(HPrz)_4Cl_2]$ was performed again in 2006 by Xing and coworkers [19], by direct treatment of copper chloride with pyrazole in a methanolic solution.

In view of the above and in continuation with its synthesis, in this study, $[Cu(HPrz)_4]Cl_2$ complex was synthesized as single crystal. The structure of the complex was characterized by FT-IR, Raman and, confirmed by single-crystal XRD studies. The graph-set descriptors of the intra- and intermolecular hydrogen bonding interactions stabilizing the title coordination compound were also reported. Although literature reveals some syntheses and experimental studies of this complex, there is lack of information on the detailed experimental and theoretical vibrational properties together with theoretical molecular structure. In addition, this research work was complemented using DFT method in conjunction with the B3LYP/6-311+G(3df,p) and B3LYP/lanl2dz levels. The highest occupied and lowest unoccupied molecular orbitals (HOMO and LUMO) of the complex were also predicted. The findings of these spectroscopic and theoretical studies are herein reported.

Experimental

Instrumentation

A dark blue block-like crystal of the complex, with dimensions of 0.10 × 0.10 × 0.15 mm was selected and mounted on an Oxford Diffraction Xcalibur CCD diffractometer with a fine-focus sealed tube graphite-monochromated Mo Kα radiation (λ = 0.71069 Å) using φ and ω scans at 170 K in the range of $2.8° \leqslant \theta \leqslant 31.7°$. The unit cell determination and data reduction were performed using the CrysAlis program [20]. A total of 8144 reflections were collected, of which 2741 were independent and 2120 reflections with $I > 2\sigma(I)$. The structure was solved by direct methods using the program SIR2008 [21] and was refined by full-matrix least squares technique on F^2 including all reflections with SHELXL-2013 program [22]. Both softwares were included within the WingX crystallographic software package [23]. All non-hydrogen atoms were anisotropically refined. All of the hydrogen atoms were located from the difference Fourier map and were fixed in calculated positions with distances constraints of C—H = 0.93 Å and N—H = 0.86 Å, and refined in riding mode with $U_{iso}(H) = 1.2\ U_{eq}$(C, N). The refinements converged at conventional *R* factor of 0.0249 and *wR* of 6.66%. Maximum and minimum peaks in the final

Table 2
Crystal data and parameters for structure refinement.

Crystal data	Complex
Empirical formula	$C_{12}\ H_{16}\ Cu\ N_{12}\ Cl_2$
Formula weight (g mol^{-1})	M_r = 406.76
Temperature (K)	170(2)
Crystal system	Monoclinic
Space group	C2/c
Unit cell dimensions (Å,°)	
a	13.5430(10)
b	9.1480(10)
c	14.6480(10)
β	116.700(5)
Volume (Å^3)	1621.3(3)
Z[a]	4
Calculated density (g/cm^3)	1.667
Absorption coefficient (mm^{-1})	1.688
F(000)	828
Crystal size (mm^3)	0.10 × 0.10 × 0.15
Color	Dark blue
Shape	Block-like crystal
Cell parameters from	8144 reflections
Wavelength (Mo Kα) (Å)	0.71073
$\theta_{max} - \theta_{min}$	31.679° − 2.791°
Measured reflections	8144
Independent reflections	2741
Reflections with $I > 2\sigma(I)$	2120
R_{int}	0.0328
Limiting indices	
h	−19 → 20
k	−13 → 11
l	−20 → 21
Refinement method	Full-matrix Least-squares on F^2
Final *R* indices [b] [$F^2 > 2\sigma(F^2)$]	
R_1, wR_2	0.0249, 0.0666
R indices (all data)	
R_1, wR_2	0.0328, 0.0685
Goodness-of-fit on F^2[c]	1.019
Data/restraints/parameters	2548/0/106
H atoms	a constrained refinement
Largest difference peak and hole (e Å^{-3})	
$\Delta\rho_{max}$, $\Delta\rho_{min}$	0.344, −0.293

[a] The asymmetric unit contains 0.5 of the chemical formula.
[b] $R_1 = \sum|Fo - Fc|/Fo$. $wR_2 = \{\sum[w(F_o^2 - F_c^2)^2]/\sum[w(F_o^2)^2]\}^{1/2}$.
[c] GOF = $\{\sum[w(F_o^2 - F_c^2)^2]/(N_{obs} - N_{var})\}^{1/2}$.

Table 1
Energetic and molecular parameters of the complex.

Parameters	B3LYP/6-311+G(3df,p)		B3LYP/lanl2dz	
	C_i	C_1	C_i	C_1
Δ*G* (Hartree)	−3466.031387	−3466.031299	−1130.673014	−1130.673018
Dipole moment (Debye)	0	0.0048	0	0.0113
Thermal total energy (kcal/mol)	199.787	199.789	201.367	201.371
Heat capacity (cal/mol K)	83.431	83.435	82.497	82.495
Entropy (kcal/mol K)	175.001	174.81	171.789	171.812
Vibrational energy (kcal/mol)	198.01	198.011	199.589	199.594
Zero point vibrational energy (kcal/mol)	184.68488	184.69229	186.51305	186.51753
Rotational constant (GHz)				
a	0.22432	0.22433	0.22298	0.22303
b	0.22331	0.22337	0.22058	0.22061
c	0.16829	0.16828	0.16693	0.16694
Relative stability (kcal/mol)	0	0.05522	0.0025	0
Mole fractions (%)	52.33	47.67	49.89	50.11

difference Fourier syntheses were 0.344 and −0.293 e Å^{-3}. Structural representations of the complex were drawn using ORTEP-3 [24] and MERCURY [25]. Analyses were carried out by the program PLATON [26], as incorporated in the WinGX [23] suite.

FT-IR spectra of the complex were recorded by KBr pellet technique in the region of 4000–400 cm^{-1} and 400–200 cm^{-1}, respectively, with Bruker Optics IFS66v/s FT-IR spectrometer at a resolution of 2 cm^{-1}. Raman spectrum in the powder form was obtained using a Bruker Senterra Dispersive Raman microscope spectrometer with 532 nm excitation from a 3B diode laser having 2 cm^{-1} resolution in the spectral region of 4000–50 cm^{-1}.

Synthesis

The title compound was obtained by mixing a warm aqueous solution of oxalic acid (10 ml, 30 °C) with a hot ethanol–water solution (1:1, 20 ml, 60 °C) of $CuCl_2$ and pyrazole in a 1:2 M ratio. On cooling to room temperature, the resulting solution was stirred for 30 min until an almost clear solution was obtained. After standard gravity filtration of any amount of insoluble material, the final solution was left at room temperature and dark-blue block-like crystals suitable for X-ray analysis appeared after few days.

Table 3
Atomic coordinates and thermal parameters (Å^2).

Atom	X	Y	Z	U_{eq}
Cu1	0.25	0.25	0.5	0.02018(7)
Cl1	0.06387(3)	0.06492(3)	0.41099(2)	0.02228(8)
N1	0.14694(9)	0.42139(11)	0.45774(8)	0.0188(2)
N4	0.33696(9)	0.34633(12)	0.35332(9)	0.0228(2)
N3	0.25973(9)	0.26925(11)	0.36706(8)	0.0180(2)
N2	0.03787(9)	0.40638(12)	0.40023(9)	0.0235(2)
C6	0.19493(11)	0.20970(15)	0.27682(10)	0.0211(3)
C5	0.23130(14)	0.24923(15)	0.20486(11)	0.0282(3)
C1	−0.01304(12)	0.53629(15)	0.37269(12)	0.0289(3)
C3	0.16542(11)	0.56453(14)	0.46628(10)	0.0228(3)
C4	0.32193(13)	0.33660(16)	0.25639(12)	0.0279(3)
C2	0.06685(12)	0.64139(15)	0.41377(12)	0.0271(3)

Computational details

All the computations were performed using the Gaussian 09 program package [27] by means of the resources provided by GridChem Science Gateway [28]. GaussView [29] was used for visualization of the structure and simulation of the vibrational spectra. The complex was optimized using the B3LYP functional in conjunction with the 6-311+G(3df,p) and lanl2dz basis sets in the gas phase imposing the C_1 and C_i symmetries. In addition, pyrazole in C_s symmetry was examined by B3LYP/6-311+G(3df,p) level of theory. Harmonic vibrational frequencies and their corresponding vibrational intensities were also computed using the same functional and basis set to confirm the nature of the stationary points. Scaling factors used in this study were taken from literature [30,31]. The fundamental normal modes were assigned. Potential energy distribution (PED) calculations were carried out by the VEDA 4 (Vibrational Energy Distribution Analysis) as described earlier [32]. Calculated Raman activities were converted to relative Raman intensities using the relationship derived from the intensity theory of Raman scattering [33,34].

Results and discussion

The crystal structure of $[Cu(HPrz)_4Cl_2]$ is explored with a discussion about the hydrogen-bonding networks and graph sets. The results of the electronic computations on the geometrical parameters of the compound are reported and discussed with respect to the X-ray data. This is followed by discussion of the experimental and theoretical vibrational frequencies, which is implemented by considering the vibrations of the pyrazole and the metal–ligand. The molecular orbitals are also searched.

Structural analyses

The energetic and some molecular parameters of the complex are listed in Table 1. For the B3LYP/6-311+G(3df,p) level, the complex in C_i symmetry is more stable than without symmetry imposition by at least 0.05 kcal/mol. The approximate percentage preference of the compound in the gas phase in the C_i symmetry

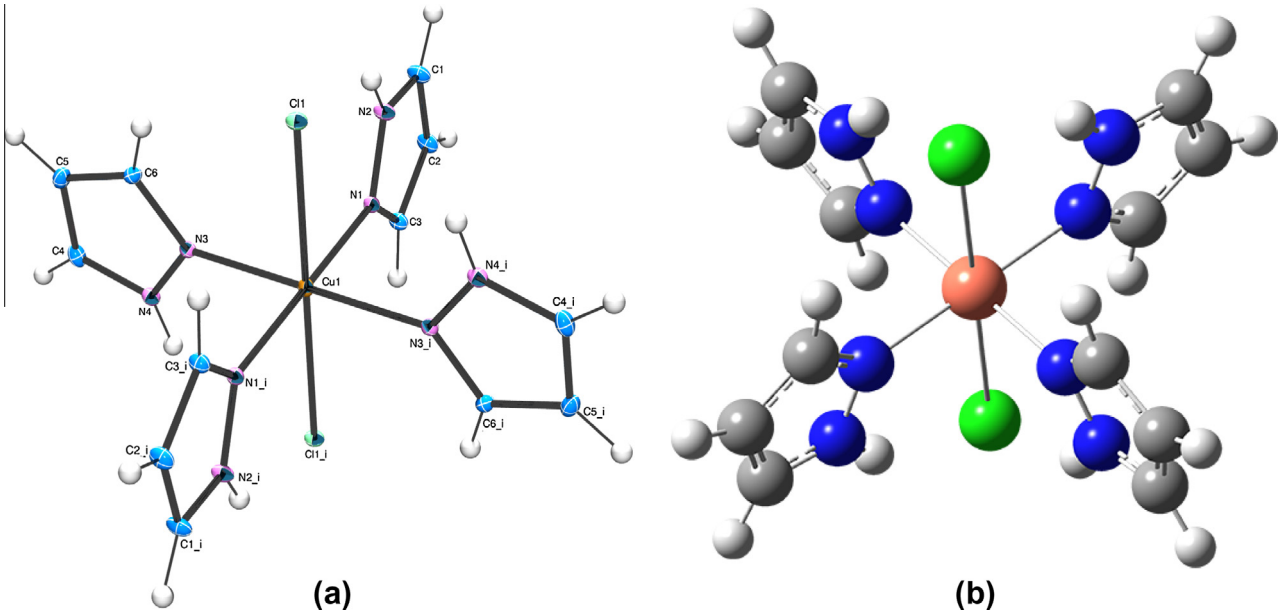

Fig. 1. (a) Molecular view of the complex showing atom labeling scheme. The thermal ellipsoids are drawn at the 30% probability level. (b) Optimized structure of the complex.

and without considering symmetry is 52% and 48%. For the B3LYP/lanl2dz level, the relative percentage of the two symmetries of the compound is about 50%. These were calculated as described in the literature [33,35]. The variation in the zero point vibrational energy is insignificant. The total energy and change in total entropy are reported at 298.15 K. It is well known that the stability decreases as the dipole moment increases. Therefore, the conformational preference of the compound can be also explained on the basis of their large dipole moments [36].

A summary of crystal data and parameters for structure refinement details are given in Table 2. The atomic coordinates and equivalent thermal parameters are also given in Table 3.

The molecular structure of the compound showing the atom-numbering scheme is shown in Fig. 1. All other refinement details are available in the CIF (CCDC: 1016199). According to data obtained, the space group and the unit cell parameters are similar to the previous results. The crystal structure, however, is determined at low temperature with a much lower *R* value (0.0249) compared to the two previously published studies (0.0488 for [18] and 0.049 for [19]). The complex crystallizes in the monoclinic space group C2/c with a centro-symmetric molecule in the asymmetric unit, formed by a half Cu^{2+} metal ion located on a center of symmetry at (¼, ¼, ½), two crystallographically independent pyrazole ligands and a chloride counter-ion located on general positions

Table 4
Some M—X and M—N bond distances of the pyrazole-derivatives complexes.

Bond	Present work	$Cu(HPrz)_4Cl_2$ [18]	$Cu(HPrz)_4Cl_2$ [19]	$Cu(HPrz)_4(ClO_4)_2$ [37]	$Cu(MPPrz)_4(ClO_4)_2$ [38]
M—X	2.8226(4)	2.839	2.8386(15)	2.4164(10)	2.520(2), 2.426(2)
M—N	2.0176(11) 2.0033(10)	2.024(3)	2.025(3)	2.0117(12)	2.002(2), 2.011(2)
		1.995(3)	2.001(3)	1.9887(11)	2.002(2), 1.994(2)
M—N (average)	2.01045	2.0095	2.013	2.0002	2.002, 2.0025
	$Mn(MePrz)_4Br_2$ [40]	$Ni(HPrz)_4Cl_2$ [41]	$Co(MPPrz)_4Cl_2$ [38]	$Ni(MPPrz)_4Cl_2$ [38]	
M—X	2.727(2)	2.507(1)	2.682(1)	2.4658(6)	
M—N	2.256(3)	2.097(2)	2.101(4)	2.107(2)	
	2.243(3)	2.087(3)	2.080(5)	2.090(2)	
M—N (average)	2.2495	2.092	2.0905	2.0985	

HPrz = Pyrazole, MePrz = 5-Methylpyrazole, MPPrz = 5-(4-methoxyphenyl)pyrazole.

Table 5
Experimental and theoretical geometric parameters.

Bond lengths (Å)	Exp.	6-311+(3df,p)	lanl2dz	Bond Angles (°)	Exp.	6-311+(3df,p)	lanl2dz
Cu1—N1	2.0033	2.048	2.041	N4—N3—Cu1	125.50	119.9	120.5
Cu1—N1	2.0033	2.048	2.041	N1—N2—C1	111.78	111.2	110.8
Cu1—N3	2.0176	2.048	2.041	N1—N2—H2N	124.10	116.6	116.2
Cu1—N3	2.0176	2.048	2.041	C1—N2—H2N	124.10	132.2	133.0
N1—C3	1.3285	1.331	1.353	N3—C6—C5	110.16	110.0	109.7
N1—N2	1.3387	1.342	1.373	N3—C6—H6	124.90	119.6	119.7
N4—C4	1.3438	1.343	1.366	C5—C6—H6	124.90	130.4	130.6
N3—N4	1.3494	1.342	1.373	C4—C5—C6	105.51	105.0	105.5
N4—H4N	0.8600	1.029	1.032	C4—C5—H5	127.20	127.4	127.1
N3—C6	1.3311	1.331	1.353	C6—C5—H5	127.20	127.6	127.4
N2—C1	1.3418	1.343	1.366	N2—C1—C2	106.99	107.2	107.2
N2—H2N	0.8600	1.029	1.032	N2—C1—H1	126.50	121.3	121.8
C6—C5	1.397	1.401	1.421	C2—C1—H1	126.50	131.5	131.0
C6—H6	0.930	1.079	1.080	N1—C3—C2	110.60	110.0	109.8
C5—C4	1.372	1.383	1.403	N1—C3—H3	124.70	119.6	119.7
C5—H5	0.930	1.077	1.079	C2—C3—H3	124.70	130.4	130.6
C1—C2	1.368	1.383	1.403	N4—C4—C5	107.05	107.2	107.2
C1—H1	0.930	1.078	1.079	N4—C4—H4	126.50	121.3	121.8
C3—C2	1.3947	1.401	1.421	C5—C4—H4	126.50	131.5	131.0
C3—H3	0.930	1.079	1.080	C1—C2—C3	105.07	105.0	105.5
C4—H4	0.930	1.078	1.079	C1—C2—H2	127.50	127.4	127.2
C2—H2	0.930	1.077	1.079	C3—C2—H2	127.50	127.6	127.4
Cu1—Cl1	2.8226	2.856	2.847				
Bond angles (°)				Torsion angles (°)			
N1—Cu1—N1^{i}	180.00	180.0	180.0	C4—N4—N3—C6	0.09	0.1	0.1
N1—Cu1—N3	88.40	89.7	89.7	C4—N4—N3—Cu1	179.33	179.1	179.0
N1^{i}—Cu1—N3	91.60	89.7	89.7	C3—N1—N2—C1	−0.32	0.1	0.0
N1—Cu1—N3^{i}	91.60	89.7	89.7	Cu1—N1—N2—C1	−173.60	−179.1	−179.0
N1^{i}—Cu1—N3^{i}	88.40	89.7	89.7	N4—N3—C6—C5	0.02	0.0	−0.1
N3—Cu1—N3^{i}	180.00	180.0	180.0	Cu1—N3—C6—C5	−179.19	−178.9	−178.9
C3—N1—N2	105.56	106.6	106.7	N3—C6—C5—C4	−0.11	0.0	−0.1
C3—N1—Cu1	131.81	133.5	132.8	N1—N2—C1—C2	0.36	−0.1	0.0
N2—N1—Cu1	122.19	119.9	120.5	N2—N1—C3—C2	0.15	0.0	0.0
C4—N4—N3	111.32	111.2	110.8	Cu1—N1—C3—C2	172.52	178.9	178.9
C4—N4—H4N	124.30	132.2	133.0	N3—N4—C4—C5	−0.16	−0.1	0.0
N3—N4—H4N	124.30	116.6	116.2	C6—C5—C4—N4	0.16	0.1	0.0
C4—N3—N4N	106.00	106.6	106.7	N2—C1—C2—C3	−0.24	0.0	0.0
C6—N3—Cu1	128.53	133.5	132.8	N1—C3—C2—C1	0.06	0.0	0.0

Symmetry codes: (i) (−*x* + ½, −*y* + ½, −*z* + 1).

(Fig. 1). The metal ions are surrounded by a slightly elongated N4Cl2 octahedral environment, formed by two N atoms from to equivalent pyrazole ligands (N1 and N1^{i}), two N atoms of two equivalent pyrazole ligands crystallographically independent from the first two (N3 and N3^{i}) and two coordinated chloride counter ions (Cl1 and Cl1^{i}, with i: (½ − x, ½ − y, 1 − z)). The four equatorial coordination sites are occupied by four N atoms belonging to the monodentately coordinated pyrazole molecules [Cu—N = 2.0033(10) and 2.0176(11) Å]. These atoms define the equatorial plane and because of the centro-symmetry, the copper ion lies in this plane. The Cu-ligand distance (average: 2.0104(2) Å) is significantly longer than the mean value observed in $[Cu(Hpz)_4SO_4](H_2O)$ of 1.944(6) Å [37]. It is comparable to those observed in other related six-coordinated copper(II)-complexes where the metal is bonded to pyrazole derivatives [18,19,38,39] (Table 4).

The two crystallographically related chloride counter ions are weakly bonded to the copper(II) center in the apical positions, with a Cu—Cl bond distance markedly longer than the equatorial ones [Cu1—Cl1 = 2.8226(4) Å]. The apical Cu—Cl distance is in agreement with those found in such six-coordinated copper(II) groups [40] with chloride counter-ions. This value is well compared with the Mn—Br bond length (2.727(2) Å) observed in the complex $Mn(MePrz)_4Br_2$ [41]. The difference between the apical and equatorial bond lengths (0.8122 Å) is slightly longer than the M—Cl observed in other metal-coordinated pyrazole derivatives complexes: 2.507(1) Å observed in the case of $Ni(HPrz)_4Cl_2$ [42], 2.4658(6) Å for $Ni(MPPrz)_4Cl_2$ [39] and 2.682(1) Å for $Co(MPPrz)_4Cl_2$ [39]. This long bond length is explained by the Jahn–Teller effect which leads to a slight decrease of the Cu—N distances, but to a pronounced decrease of the Cu—Cl bond distance.

The crystallographically different pyrazole rings in the basal plane around the copper ion are in trans arrangement in respect of each other. Therefore, they are disposed in an orthogonal way in comparison with the N_4Cu plane. All the structural parameters within the ligand lie in usual ranges (Table 5) and compare well with the pyrazole-derivative complexes previously reported [41,43] except for the C1—N2 (1.3418(17) Å), N3—N4 (1.3494(15) Å) and C4—C5 (1.372(2) Å) bond distances which are slightly longer than those reported in the case of catena-Poly[[tetrakis(1H-pyrazole-κN^2)-copper(II)]-μ-hexafluoridosilicato-κ^{2}F:F′] (1.324(6), 1.332(5) and 1.350(7) Å, respectively) [44]. The pyrazole rings are planar and the largest deviations of atoms from the mean plane are 0.0022 Å or 0.0011 Å. Their mean planes are at 83.47° to each other and at 87.63° and 89.83° to the equatorial plane containing the nitrogen atoms (N1, N1^{i}, N3 and N3^{i}). The highest torsion angle within the pyrazole ligand, N1—N2—C1—C2, has the value of 0.36(17)°. The crystallographic analysis of the complex also revealed that the shortest Cu···Cu distance through the [100] direction is 8.1716(5) Å. The thiocyanate mononuclear-copper complex $[Ni(pzph)_4(NCS)_2]$ (Pz^{ph} = 3-phenylpyrazole) [45] exhibits a similar M···M separation of 8.591 Å.

To clarify the vibrational frequencies, it is essential to examine the geometry of the compound. A slight change in the geometry can potentially cause substantial variations in their frequencies. Some of the experimental and theoretical (optimized) geometric parameters (bond lengths, bond angles and torsion angles) are listed in Table 5.

In general, all the calculated parameters are in good agreement with the reported experimental data. Regarding the calculations, the largest difference between the experimental and calculated bond lengths, bond angles and torsion angles for C_i symmetry with the lanl2dz are 0.172 Å (N—H), 8.1° (C—N—H) and 6.38° (Cu—N—C—C). The corresponding values for the 6–311+(3df,p) basis set are 0.169 Å, 8.9° and 6.38°. The root mean square

Table 6
Hydrogen bond lengths (Å) and angles (°).

D—H···A	D—H	H···A	D···A	D—H···A
N2—H2N···Cl1	0.8600	2.4700	3.1395(11)	135
N4—H4N···Cl1$^{(i)}$	0.8600	2.7800	3.4385(13)	135
N4—H4N···Cl1$^{(ii)}$	0.8600	2.5600	3.1961(12)	131

Symmetry codes: (i) $x + ½, y + ½, z$; (ii) $-x + ½, -y + ½, -z + 1$.

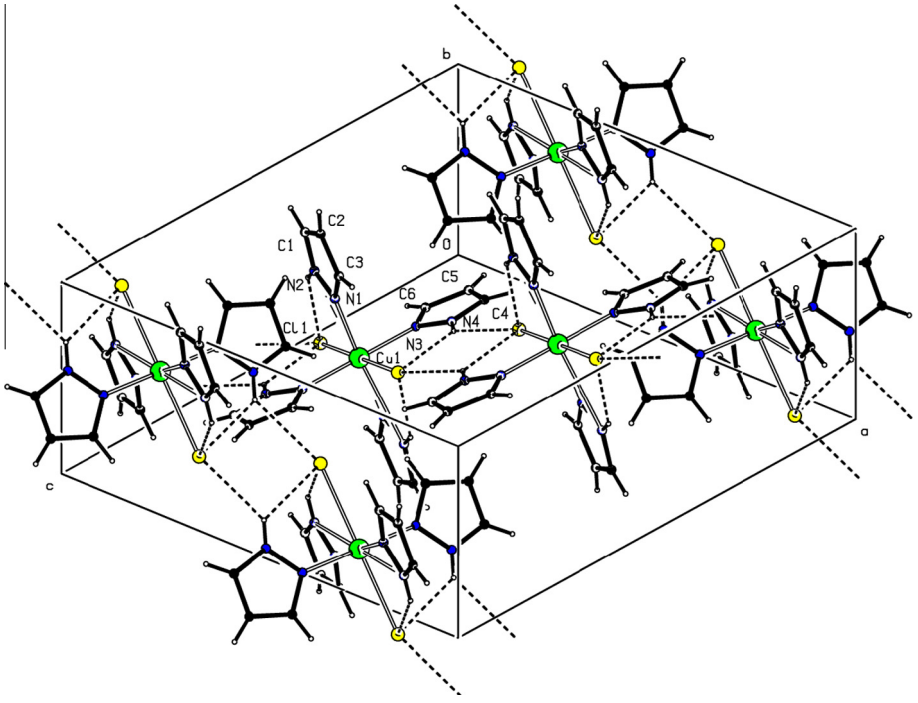

Fig. 2. Crystal packing of the complex showing the H-bonding patterns.

deviation (RMSD) and the mean absolute deviation (MAD) between the experimental and calculated bond lengths, bond angles and torsion angles are found to be 0.094 Å – 0.072 Å, 3.906° – 2.728° and 2.248° – 1.007° for lanl2dz and 0.092 Å – 0.063 Å, 3.881° – 2.750° and 2.266° – 1.007° for 6-311+(3df,p), respectively.

Graph-sets of hydrogen bonding

The crystal packing of the complex are mainly consolidated by N—H···Cl intra and intermolecular hydrogen bonds. Therefore, a total of three counter-ion-ligand hydrogen bonds are present in the asymmetric unit (Table 6). Each chloride counter-ion of this complex is doubly hydrogen-bonded to two N atoms of the ligand (N4 and N2) yielding to intramolecular contacts on the one hand and, to another ligand nitrogen N4 belonging to a neighboring molecule (3.4385(13) Å) on the other hand. Hence, the counter-ions act as a four-centered interaction acceptors. A three-centered hydrogen bond is built of the non-coordinated N4 atom as a double-donor and two chlorides (Fig. 2). Besides, being the acceptors of N—H···Cl hydrogen bonds, the Cl counter-ions atoms form quite close Cl···Cl type interactions with their symmetry equivalents from the adjacent molecule. The shortest intermolecular Cl···Cl distance is found to be equal to 3.906 Å.

In the crystal packing, each copper complex is connected to two adjacent discrete molecules through pairs of N4—H4N···Cl1 hydrogen bonds of 3.438(1) Å in such a way to give infinite one-dimensional C(5) [46] double ribbons in the (ac) plane. An ample view of the packing proves that the centro-symmetric $R_2^2(10)$ rings illustrate how the neighboring moieties link to each other through the N4—H4N···Cl1 interaction. These rings are connected together by the metallic center Cu1, yielding to infinite supramolecular center-fused cycles (Fig. 3a). The intramolecular N2—H2N···Cl1 interaction enhances a primary graph-set formed essentially by a $D_2^2(9)$ descriptor. Each $D_2^2(9)$ dimer is linked through the copper-center to yield two center-fused R(5) five-membered rings. Furthermore, the N4 atom is involved in a N4—H4N···Cl1 hydrogen bonding of 3.139(1) Å which self-assemble forming a $D_2^2(7)$ dimer and two R(5) rings linked together through the copper metallic cation (Fig. 3b).

The C(5) infinite ribbons are packed in the crystal lattice and linked to each other by intramolecular interactions (3.196(1) Å) involving the non-coordinated doubly-donor N4 atoms where their combination generate $R_2^2(6)$ binary-level cycles. Together with the two linked R(5) rings take part in building an alternating edge-fused and center-fused cycles giving rise to infinite sheets (Fig. 4) running through the (ac) plane. Furthermore, a $C_2^1(8)$ secondary-level graph-set are observed when combining the intermolecular N4—H4N···Cl1

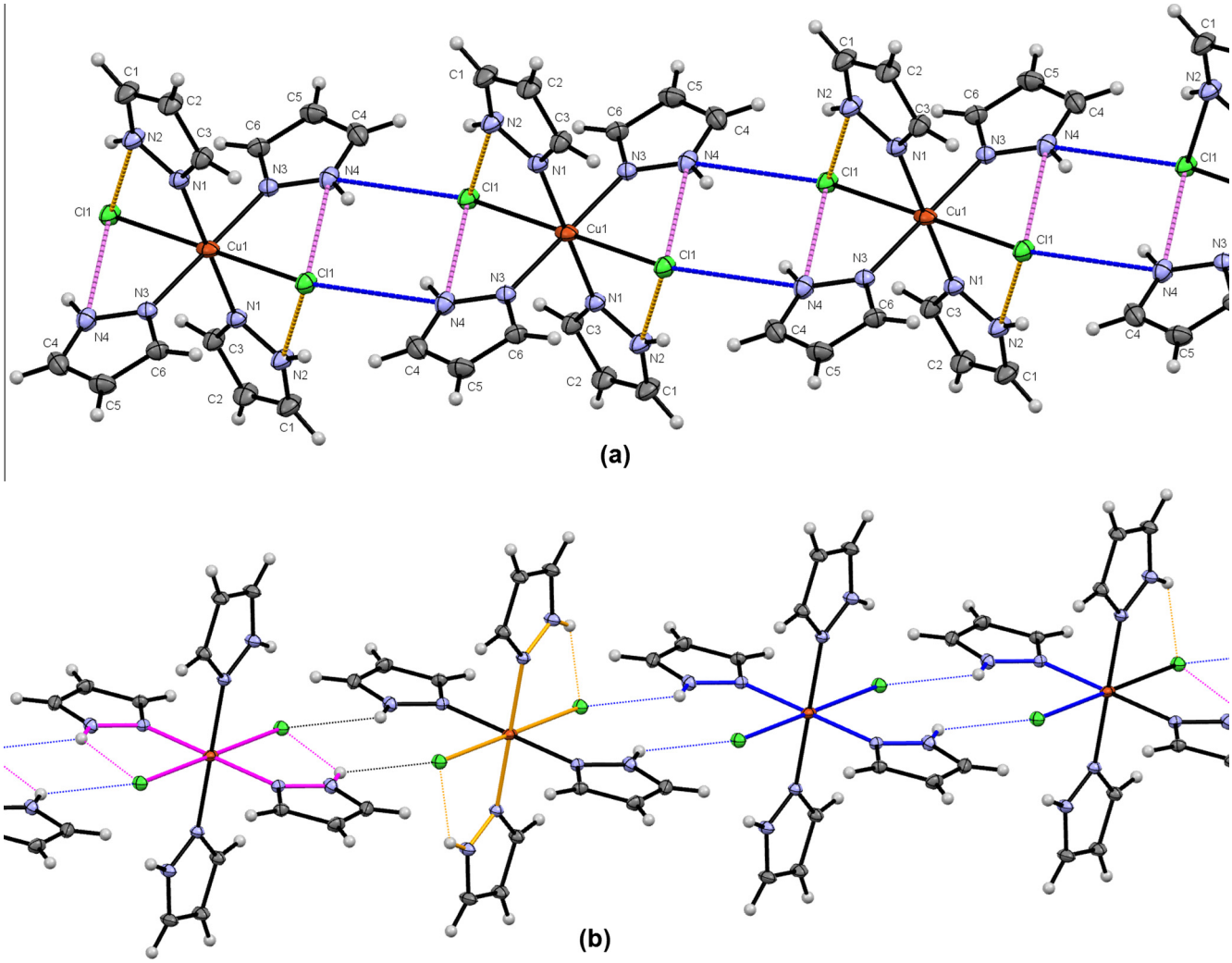

Fig. 3. (a) A crystal structure view of the complex illustrating how the discrete moieties link to each other through the N—H···Cl interactions. (b) A fragment of the structure showing the first-level graph set descriptors with hydrogen bonds as dashed lines (C(5) and $R_2^2(10)$ are given in blue, $D_2^2(9)$ and R(5) are drawn with orange, $D_2^2(7)$ and R(5) are in purple). Some of the H-bonds were omitted for clarity. (For interpretation of the references to color in this figure legend, the reader is referred to the web version of this article.)

interaction together with N2—H2N···Cl1 generating double-ribbons. These ribbons are linked by the metallic center resulting in copper-center-connected $R_4^2(16)$ rings. The association of the three alternating N—H···Cl interactions yields to a ternary-level graph set which can be described as polymeric $C_2^2(8)$ layers.

Vibrational studies

Pyrazole ligand molecule consists of 9 atoms, having 21 normal vibrational modes, and it belongs to the point group C_s. The 21 modes of vibrations account for the irreducible representations $\Gamma_v = 15A' + 6A''$ of the C_s point group. There are some published reports about its vibrational spectra [47–52]. All the experimental and theoretical vibrational frequencies of pyrazole observed in the vibrational spectra of the complex, along with corresponding vibrational assignments and intensities are given in Table 7. The experimental and simulated (C_i symmetry) vibrational spectra of the complex are depicted in Figs. 5 and 6. As can be seen from Table 7 and Figs. 5 and 6, the spectral data for pyrazole in the complex exhibit characteristics of a coordinated ligand. As evident from Table 7, considerable shifts to higher or lower frequencies occur for some absorption bands in the spectra of the complex.

The following are important vibrational shifts that were observed: the IR band at 3523 cm^{-1} for free pyrazole is assigned to the NH stretching mode. For the complex, this mode is observed at 3205 cm^{-1} in the IR spectrum. The corresponding theoretical value is computed at 3174 cm^{-1}. CH stretching vibrations are observed at 3155/3150, 3137/3132 and 3126/3119 (IR/R) cm^{-1}. These bands are shown as 3146/3112 cm^{-1} in the present complex. The corresponding theoretical values of these modes are computed

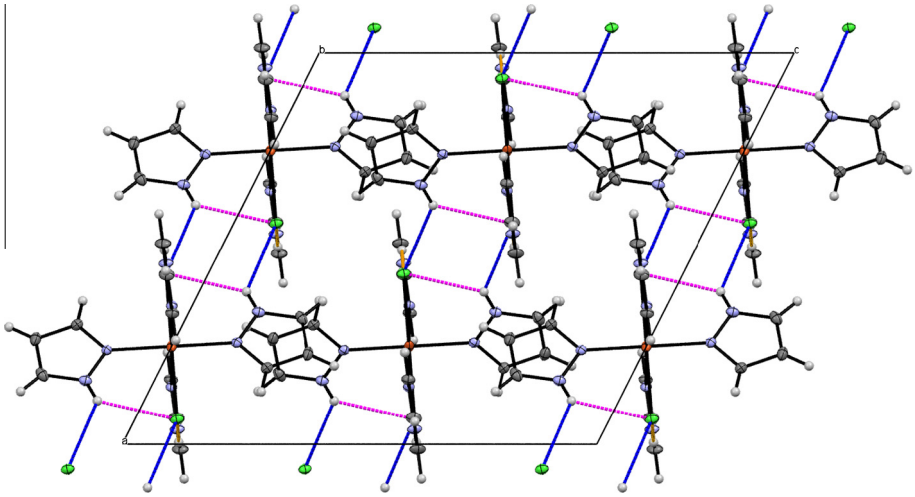

Fig. 4. Projection through the (ac) plane showing the binary-level graph-sets built from rings.

Table 7
Vibrational wavenumbers (cm^{-1}) of pyrazole vibrations in the present complex.

Assignments[a] PED (⩾10%)[b]	Pyrazole					Complex							
	B3LYP/6-311+(3df,p)			Experimental[d]		B3LYP/6-311+(3df,p)			B3LYP/lanl2dz			Experimental	
	ν*	I_{IR}[c]	I_R[c]	IR	Raman	ν*	I_{IR}[c]	I_R[c]	ν**	I_{IR}[c]	I_R[c]	IR	Raman
νNH(100)	3551	85.64	14.28	3523	–	3174	464.69	46.66	3200	46.66	47.70	3205	–
νCH(93)	3164	0.34	26.50	3155	3150	3161	9.25	13.38	3184	13.38	6.68	–	3146
νCH(88)	3147	1.20	7.80	3137	3132	3151	170.87	6.02	3173	6.02	4.30	–	–
νCH(97)	3133	2.82	17.85	3126	3119	3143	115.96	21.79	3165	21.79	25.53	3112	–
νCC(46), δCH(21), νNC(20)	1515	6.31	1.54	1531	1538	1516	11.84	2.81	1490	2.81	2.78	1513	1513
νNC(58), δNH(30)	1431	6.66	1.86	1447	1476	1470	27.28	2.62	1435	2.62	4.40	1474/1466	1468
νCC(55), δCH(35)	1375	12.67	12.28	1395	1399	1392	22.13	10.25	1381	10.25	16.35	1394	1410
νNN(51), νCC(26), δCH(15)	1341	5.07	9.26	1358	1356	1350	28.20	13.84	1331	13.84	9.73	1359/1349	1355
δCH(53), νNN(23), νCC(20)	1241	2.11	12.86	1254	1260	1265	5.96	12.23	1258	12.23	13.75	1268/1253	1265
νCC(55), νNN(27), δNH(10)	1141	0.24	25.56	1159	1151	1159	20.85	25.74	1141	25.74	7.78	1166	1165
νNC(66), νCC(15), δNH(10)	1106	21.18	5.41	1121	1138	1129	45.51	10.58	1119	10.58	32.80	1126/1117	1116
δCH(53), νCC(26)	1021	5.97	1.99	1054	1050	1044	58.89	1.64	1043	1.64	3.96	1073	1063
δCH(49), νNN(30)	1014	37.04	1.69	1009	1038	1031	14.46	2.68	1020	2.68	1.58	1046	–
δ-ring(86)	913	4.60	0.96	924	930	928	21.29	11.05	924	11.05	5.11	944	945
δ-ring(88)	896	9.51	2.07	908	915	906	3.79	2.67	918	2.67	7.22	911	–
ωCH(93)	873	5.69	0.13	879	867	904	3.27	1.65	900	1.65	8.17	902	–
ωCH(94)	824	6.24	1.57	833	834	859	11.82	0.81	887	0.81	5.63	866	862
ωCH(88)	732	96.47	0.90	745	772	794	49.16	0.77	832	0.77	3.01	777/759	–
t-ring(84)	669	17.59	0.15	674	657	745	37.61	1.83	765	1.83	1.17	713	698
t-ring(89)	620	0.17	0.07	623	612	648	1.86	0.21	643	0.21	0.17	655	647
t-ring(73), ωNH(14)	513	55.61	0.24	516	–	608	7.18	0.21	607	0.21	1.59	613/598	–

ν* and ν**: Scaled frequency with 0.9683 and 0.9610, respectively. ν, δ, ω and t denote stretching, in plane bending, wagging and twist, respectively.
[a] Assignments for complex.
[b] PED data are taken from VEDA4.
[c] I_{IR} and I_R: Calculated infrared (km/mol) and Raman (Å/amu) intensities.
[d] Ref. [50].

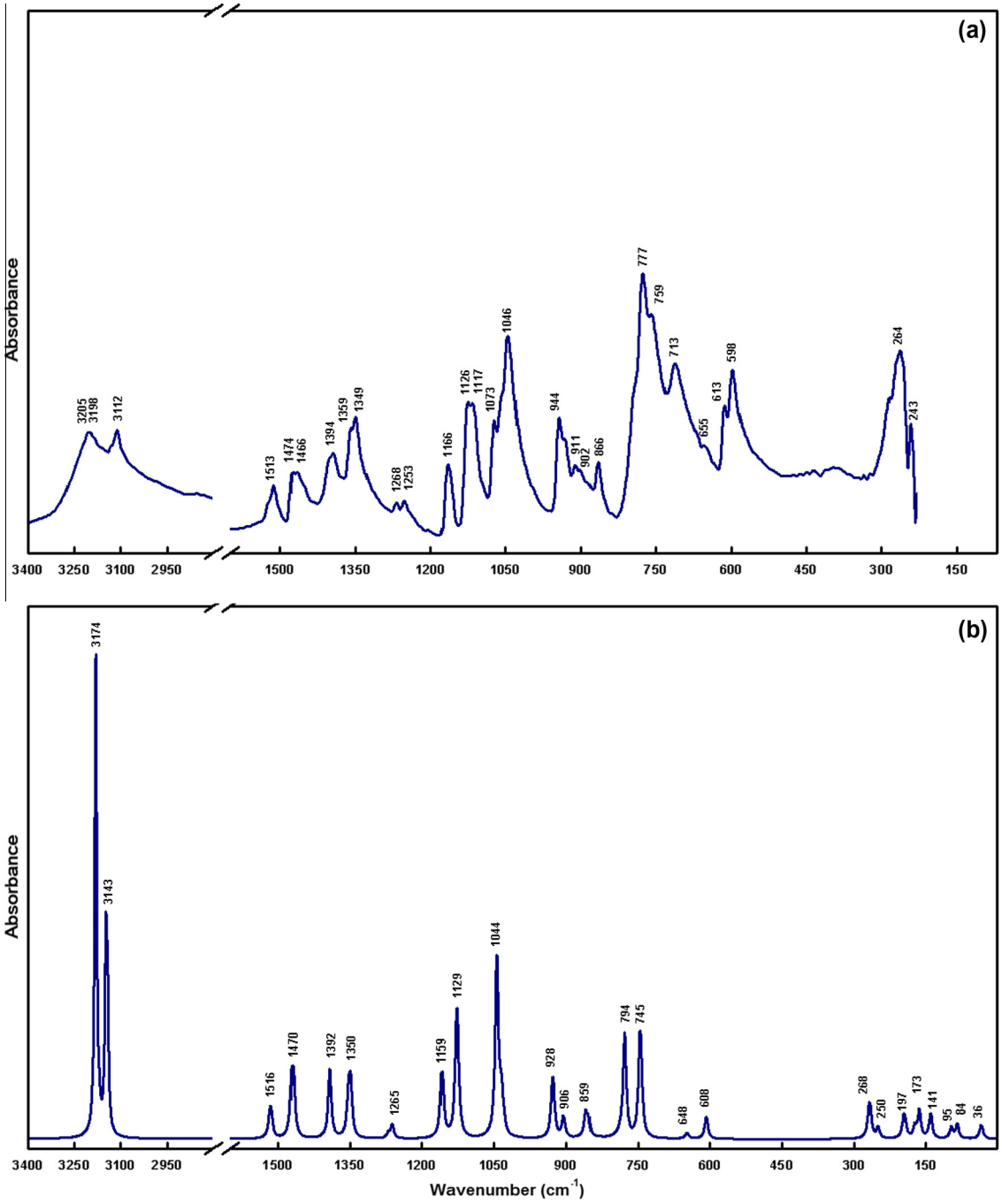

Fig. 5. (a) Experimental and (b) theoretical IR spectra of the complex.

at 3161, 3151 and 3143 cm^{-1}. R/IR bands observed at 1538/1531 cm^{-1} for free ligand are assigned to ring stretching. This vibration is shifted to downward approximately 22 cm^{-1} when compared with the complex. This mode is calculated at 1516 cm^{-1}. Vibrational spectra of the complex may be affected from N—H···Cl interactions. Therefore, these shifts may be attributed to N—H···Cl interactions in the complex.

The vibrational wavenumbers of pyrazole in the complex show other red-shifts and blue-shifts when compared with the free molecule, and these shifts are metal dependent. The IR/R bands at 1447/1476, 1358/1356 and 1121/1138 cm^{-1} are assigned to the ring stretching vibrations (C—N, N—N and C═N, respectively). On coordination, there are some increases or decreases and splittings for these frequencies: 1474/1466/1468, 1359/1349/1355 and 1126/1117/1116 (IR/IR/R) cm^{-1}. The computed data for these modes are 1470, 1350 and 1129 cm^{-1}, respectively. The reason of the splittings detected on the IR spectrum of the complex is thought as it is revealed as a result of the Jahn–Teller degeneration effect [53,54]. It might be understood, from the presence of this effect in the complex, that the rings surrounding Cu(II) ion have two unequal Cu—N bonding couples in different lengths. When the CN or NN stretching vibrations, are splitted in two levels in IR spectra of the complex, the peak at the lower frequency seems to be the result of the longer Cu—N bond. These spectral data are in good agreement with the structural data presented. These splittings have been observed in the previous studied complexes : Cu(cyclam)$M(CN)_4$

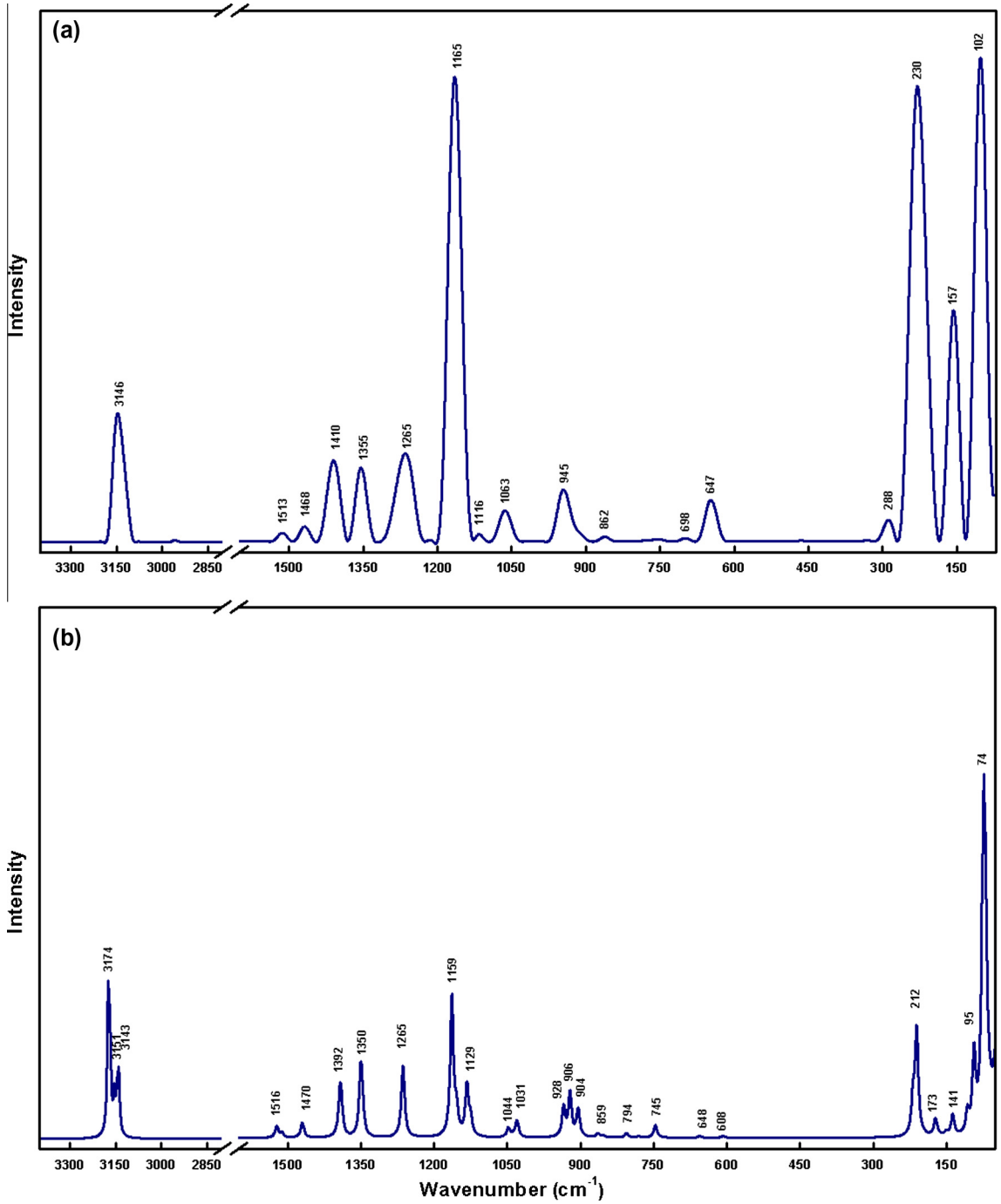

Fig. 6. (a) Experimental and (b) theoretical Raman spectra of the complex.

[55] (with cyclam = 1,4,8,11-tetraazacyclotetradecane and M = Ni, Pd, Pt), $[Cu(mim)_2Pd(CN)_4]_n$ [56] (mim = 2-methylmidazole) and $[M(sac)_2(pz)_2(H_2O)_2]$ [57] (with sac = saccharin and pz = pyrazole). As well as the strong shifts, another spectral feature caused by coordination is the small frequency shifts resulting from the environmental changes of pyrazole. All observed shifts of the vibrational frequencies are consistent with other previous studies [58,59].

The experimental and theoretical vibrational wavenumbers of the metal–ligand vibrations in the present complex are listed in Table 8. The Cu—N stretching, in plane bending and out of plane bending vibrations are observed at 264 (IR)/288 (R), 243 (IR) and 102 (R) cm^{-1} whereas the Cu—Cl stretching and out of plane bending vibrations are assigned as 230 (R) and 157 (R) cm^{-1}. The corresponding theoretical values of these modes are found to be 268, 250, 95 and 212, 141 cm^{-1}, respectively. All observed bands for the low region are consistent with other previous studies [59,60]. Furthermore, in general, the computed frequencies are in excellent agreement with the experimental data.

Molecular orbital analysis

The HOMO–LUMO analyze has been carried out to visualize frontier molecular orbitals and examine charge transfer within the complex and the energy difference called as energy gap between HOMO and LUMO orbitals. This amount of energy is described by one electron excitation from HOMO to LUMO orbitals

Table 8
Vibrational wavenumbers (cm^{-1}) of the metal–ligand vibrations in the present complex.

Complex								
Assignments[a] PED (⩾10%)[b]	Experimental		B3LYP/6-311+(3df,p)			B3LYP/lanl2dz		
	IR	Raman	ν^*	I_{IR}[c]	I_R[c]	ν^{**}	I_{IR}[c]	I_R[c]
νCuN(92)	264	288	268	26.1	0	280	27.17	0
δCuN(83), νCuCl(10)	243	–	250	13.91	0	257	15.46	0
νCuCl(91)	–	230	212	0	105.64	215	0	54.62
νCuCl(86)	–	–	197	26.87	105.6	209	23.95	54.62
γCuN(81)	–	–	173	14.12	8.2	172	21.95	15.96
γCuCl(90)	–	157	141	31.23	20.62	144	23.77	26.06
γCuN(50), νCuCl(42)	–	102	95	14.27	6.87	106	31.5	9.59
γCuN(56), νCuCl(33)	–	–	84	17.79	73.52	97	5.36	56.22
γCuN (71), νCuCl(18)	–	–	74	0	226.96	73	0	404.8
δCuN(75), δCuCl(17)	–	–	36	7.95	2218	38	3.89	2619

ν^* and ν^{**}: Scaled frequency with 0.9683 and 0.9610, respectively. ν, δ and γ denote stretching, in plane bending and out of plane bending, respectively.
[a] Assignments for complex.
[b] PED data are taken from VEDA4.
[c] I_{IR} and I_R: Calculated infrared (km/mol) and Raman (Å/amu) intensities.

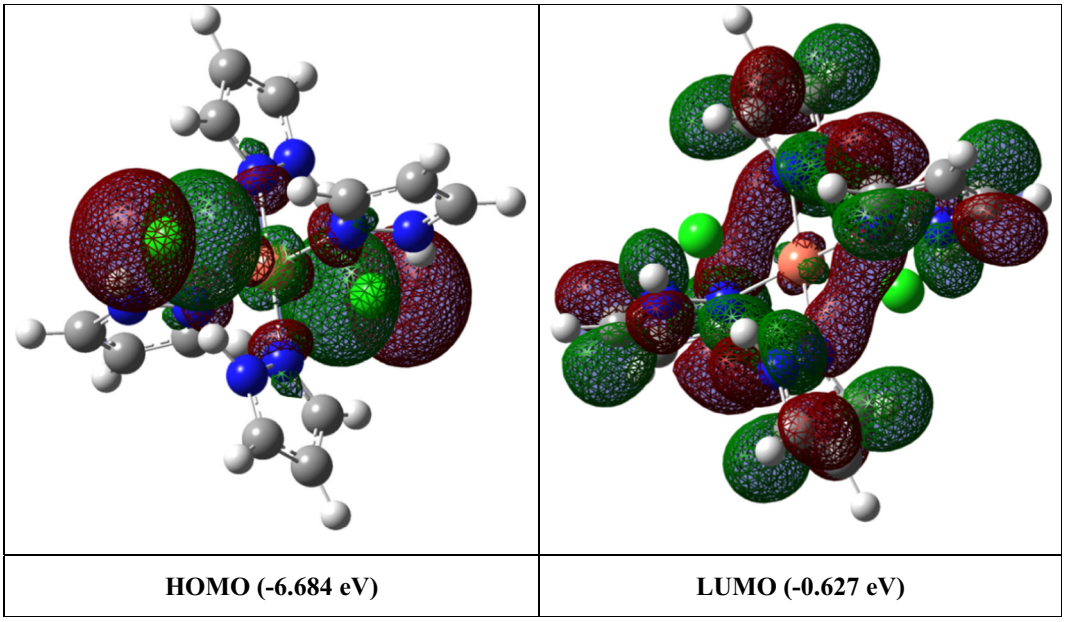

Fig. 7. HOMO and LUMO of the complex.

and corresponds to electronic absorption energy. The density plot of the HOMO and LUMO for the C_i symmetry of the title compound is shown in Fig. 7. These diagrams were plotted with a contour value of 0.02. It can be observed from Fig. 7 that the calculated HOMO orbital is delocalized on the Cu coordinated part whereas the LUMO orbital is delocalized on the pyrazole ligand in the complex. According to the calculation, the charge transfer occurs from the Cu coordinated part to the ligand molecules within the complex. The HOMO–LUMO gap is observed to be 6.057 eV, which is sufficiently large to meet the viability criterion suggested by Hoffmann et al. [61].

Conclusions

The experimental, theoretical structural and vibrational investigations of an octahedral copper(II) complex with pyrazole ligands were successfully performed by FT-IR, Raman, single-crystal XRD and quantum chemical computations. Any differences observed between the experimental and computed values may be due to the fact that the computations were performed for a single molecule in the gas phase, whereas the experimental values in the solid phase were recorded in the presence of intermolecular interactions. To summarize, the following conclusions can be drawn:

1. The complex crystallizes in the monoclinic system, space group C2/c with a centro-symmetric molecule in the asymmetric unit.
2. The C_i symmetry is more stable than the C_1 symmetry for the present complex.
3. Crystal of the complex reveals a slightly distorted octahedral geometry around the Cu(II) centers. The equatorial plane is formed by four N atoms of the four monodentately pyrazole ligands. Two symmetry-related chloride counter-ions occupy the axial positions whereas the crystallographically different pyrazole rings in the basal plane around the copper ion are trans to one another.
4. The structure is held together through N—H···Cl hydrogen bonds occurring between the coordinated pyrazole molecules and the chloride counter-ions and resulting in five-membered infinite chains.

5. The coordination sphere of copper atoms of complex displays deformation due to the Jahn–Teller effect.
6. As considering lanl2dz basis set, large MAD and RMSD values (IR/R) are found as 46.86/37.82 and 62.70/54.74 cm^{-1} for the computed raw vibrational frequencies. After scaling factors, these values decrease and are found to be 21.33/21.06 and 27.43/26.07 cm^{-1}. For the 6-311+G(3df,p) basis set, these values are equal to 37.57/33.53 and 46.90/40.64 cm^{-1} for the raw data and 11.48/12.35 and 15.86/16.61 cm^{-1} for the scaled values.
7. The B3LYP/6-311+G(3df,p) computation is better than the B3LYP/lanl2dz. Therefore, it is reliable and complement in understanding the vibrational spectra and structural parameters of the investigated compound.

Acknowledgements

AD acknowledges Dr. Triki from University of Brest for providing diffraction facilities and Université Abbes Laghrour for financial support. CP and MT acknowledge the facilities from Dumlupinar University.

Appendix A. Supplementary data

CCDC No. 1016199 contains the supplementary crystallographic data for this paper. The data can be obtained via www.ccdc.cam.ac.uk/datarequest/cif by e-mailing data_request@ccdc.cam.ac.uk or by contacting the Cambridge Data Cente, 12 Union Road, Cambridge, CB2IEZ, UK. Supplementary data associated with this article can be found, in the online version, at http://dx.doi.org/10.1016/j.molstruc.2015.03.068.

References

[1] V. Montoya, J. Pons, J. Garcia-Antón, X. Solans, M. Font-Bardia, J. Ros, Inorg. Chim. Acta 360 (2007) 625–637.
[2] T. Itoh, Y. Fuji, T. Toda, Bull. Chem. Soc. Jpn. 69 (1996) 1265.
[3] Y.J. Sun, P. Cheng, S.P. Yan, D.Z. Liao, Z.H. Jiang, P.W. Shen, J. Coord. Chem. 55 (2002) 363.
[4] S. Trofimenko, Prog. Inorg. Chem. 34 (1986) 115–210.
[5] M.K. Ehlert, S.J. Rettig, A. Storr, R.C. Thompson, J. Trotter, Can. J. Chem. 70 (1992) 1121–1128.
[6] M.H.W. Lam, Y.Y. Tang, K.M. Fung, X.Z. You, W.T. Wong, Chem. Commun. (1997) 957–958.
[7] T.N. Sorrell, V.A. Vankai, M.L. Garrity, Inorg. Chem. 30 (1991) 207–210.
[8] A. Togni, L.M. Venanzi, Angew. Chem. Int. Ed. Engl. 33 (1994) 497–526.
[9] A. Gürsoy, S. Demiryak, G. Çapan, K. Erol, K. Vural, Eur. J. Med. Chem. 35 (2000) 359–364.
[10] D.E. Lynch, I. McClenaghan, Acta Cryst. E 61 (2005) o2349–o2351.
[11] D. Crawford, A.K. Hofer, K.L. Edler, G.M. Ferrence, Acta Cryst. E 67 (2011) 496.
[12] V.G. Pacios, M. Arroyo, N. Anton, D. Miguel, F. Villafañe, J. Chem. Soc. Dalton Trans. (2009) 2135–2141.
[13] (a) J. Klingele, S. Dechert, F. Meyer, Coord. Chem. Rev. 253 (2009) 2698–2741; (b) A. Sachse, S. Demeshko, S. Dechert, V. Daebel, A. Lange, F. Meyer, Dalton Trans. (2010) 3903–3914; (c) G. Noël, J. Röder, S. Dechert, H. Pritzkow, L. Bolk, S. Mecking, F. Meyer, Adv. Synth. Catal. 348 (2006) 887–897.
[14] (a) M. Stollenz, H. Gehring, V. Konstanzer, S. Fischer, S. Dechert, C. Grosse, F. Meyer, Organometallics 30 (2011) 3708–3725; (b) L.K. Frensch, K. Pröpper, M. John, S. Demeshko, C. Brückner, F. Meyer, Angew. Chem. 123 (2011) 1456–1460.
[15] (a) O. Kahn, C.J. Martinez, Science 279 (1998) 44–48; (b) J. Olguín, S. Brooker, Coord. Chem. Rev. 255 (2011) 203–240; (c) J. Olguín, S. Brooker, New J. Chem. 35 (2011) 1242–1253.
[16] (a) J. Reedijk, Recl. Trav. Chim. Pays-Bas 88 (1969) 1451–1470; (b) J. Reedijk, Inorg. Chim. Acta 3 (1969) 517–522; (c) J. Reedijk, Recl. Trav. Chim. 89 (1970) 605; (d) J. Reedijk, Recl. Trav. Chim. 89 (1970) 993–1016; (e) J. Reedijk, Proc. Int. Conf. Coord. Chem. 13 (1970) 189; (f) J. Reedijk, Recl. Trav. Chim. 90 (1971) 117–129.
[17] A. Mighell, A. Santoro, E. Prince, C. Reimann, Acta Cryst. B 31 (1975) 2479–2482.
[18] Y.J. Sun, P. Cheng, S.P. Yan, D.Z. Liao, Z.H. Jiang, P.W. Shen, J. Mol. Struct. 597 (2001) 191–198.
[19] Y.H. Xing, J. Han, B.L. Zhang, X.J. Zhang, Y.H. Zhang, G.H. Zhou, Acta Cryst. E 62 (2006) m3354–m3356.
[20] CrysAlis CCD, CrysAlis RED and Associated Programs: Oxford Diffraction, Oxford Diffraction Ltd., Abingdon, England, 2006.
[21] SIR2008 & IL MILIONE: M.C. Burla, R. Caliandro, M. Camalli, B. Carrozzini, G.L. Cascarano, L. De Caro, C. Giacovazzo, G. Polidori, D. Siliqi, R. Spagna, J. Appl. Cryst. 40 (2007) pp. 609–613.
[22] G.M. Sheldrick, Acta Crystallogr. A 64 (2008) 112–122.
[23] WinGX: L.J. Farrugia, J. Appl. Cryst. 45 (2012) pp. 849–854.
[24] L.J. Farrugia, J. Appl. Cryst. 45 (2012) 849–854.
[25] I.J. Bruno, J.C. Cole, P.R. Edgington, M. Kessler, C.F. Macrae, P. McCabe, J. Pearson, R. Taylor, Acta Cryst. B 58 (2002) 389–397.
[26] A.L. Spek, Acta Cryst. D 65 (2009) 148–155.
[27] M.J. Frisch, G.W. Trucks, H.B. Schlegel, G.E. Scuseria, M.A. Robb, J.R. Cheeseman, G. Scalmani, V. Barone, B. Mennucci, G.A. Petersson, H. Nakatsuji, M. Caricato, X. Li, H.P. Hratchian, A.F. Izmaylov, J. Bloino, G. Zheng, J.L. Sonnenberg, M. Hada, M. Ehara, K. Toyota, R. Fukuda, J. Hasegawa, M. Ishida, T. Nakajima, Y. Honda, O. Kitao, H. Nakai, T. Vreven, J.A. Montgomery Jr., J.E. Peralta, F. Ogliaro, M. Bearpark, J.J. Heyd, E. Brothers, K.N. Kudin, V.N. Staroverov, R. Kobayashi, J. Normand, K. Raghavachari, A. Rendell, J.C. Burant, S.S. Iyengar, J. Tomasi, M. Cossi, N. Rega, J.M. Millam, M. Klene, J.E. Knox, J.B. Cross, V. Bakken, C. Adamo, J. Jaramillo, R. Gomperts, R.E. Stratmann, O. Yazyev, A.J. Austin, R. Cammi, C. Pomelli, J.W. Ochterski, R.L. Martin, K. Morokuma, V.G. Zakrzewski, G.A. Voth, P. Salvador, J.J. Dannenberg, S. Dapprich, A.D. Daniels, Ö. Farkas, J.B. Foresman, J.V. Ortiz, J. Cioslowski, D.J. Fox, Gaussian 09, Revision A.01, Gaussian, Inc., Wallingford CT, 2009.
[28] R. Dooley, K. Milfeld, C. Guiang, S. Pamidighantam, G. Allen, J. Grid. Comput. 4 (2006) 195–208.
[29] R.D. Dennington, T.A. Keith, J.M. Millam, GaussView 5.0.8, Gaussian Inc., 2008.
[30] J.P. Merrick, D. Moran, L. Radom, J. Phys. Chem. 111 (2007) 11683–11700.
[31] R.D. Johnson III, NIST computational chemistry comparison and benchmark database, NIST Standard reference database number 101, http://cccbdb.nist.gov/, (16.08.13).
[32] M.H. Jamróz, Spectrochim. Acta A 114 (2013) 220–230.
[33] Ö. Alver, C. Parlak, Vib. Spectrosc. 54 (2010) 1–9.
[34] M. Tursun, G. Keşan, C. Parlak, M. Şenyel, Spectrochim. Acta A 114 (2013) 668–680.
[35] C. Parlak, J. Mol. Struct. 966 (2010) 1–7.
[36] C.L. Perrin, D.B. Young, Tetrahedron Lett. 36 (1995) 7185–7188.
[37] W.Z. Shen, L. Yi, P. Cheng, S.P. Yan, D.Z. Liao, Z.H. Jiang, Inorg. Chem. Commun. 7 (2004) 819–822.
[38] F.T. Edelmann, D.E. Kaufmann, S. Blaurock, T. Wagner, V. Zapol'skii, Acta Cryst. E 64 (2008) m1315.
[39] S. Bergner, G. Wolmershäuser, H. Kelm, W.R. Thiel, Inorg. Chim. Acta 361 (2008) 2059–2069.
[40] M. Malecka, L. Checinska, Acta Cryst. C 59 (2003) m115–m117.
[41] J. Reedijk, B.A. Stork-Blaisse, G.C. Verschoor, Inorg. Chem. 10 (1971) 2594–2599.
[42] C.W. Reimann, A.D. Mighell, F.A. Mauer, Acta Cryst. 23 (1967) 135–141.
[43] M. Seredyuk, M. Haukka, V.A. Pavlenko, I.O. Fritsky, Acta Cryst. E 65 (2009) m1396.
[44] H. Li, Q. Han, X. Chai, J. Wang, C. Yao, Acta Cryst. E 68 (2012) m405.
[45] Y.J. Sun, X.Y. Chen, P. Cheng, S.P. Yan, D.Z. Liao, Z.H. Jiang, P.W. Shen, J. Mol. Struct. 613 (2002) 167–173.
[46] (a) M.C. Etter, Chem. Res. 23 (1990) 120–126; (b) M.C. Etter, J. Phys. Chem. 95 (1991) 4601–4610.
[47] A. Zecchina, L. Cerruti, S. Coluccia, E. Borello, J. Chem. Soc. B (1967) 1363–1368.
[48] S.T. King, J. Phys. Chem. 74 (1970) 2133–2138.
[49] (a) V. Tabacik, Hs.H. Gunther, J. Mol. Spectrosc. 45 (1973) 316; (b) V. Tabacik, Hs.H. Gunther, J. Mol. Spectrosc. 45 (1973) 319.
[50] V. Tabacik, V. Pellegrin, Spectrochim. Acta A 35 (1979) 1055–1081.
[51] M. Majoube, J. Raman Spectrosc. 20 (1989) 49–60.
[52] J.R. Durig, M.M. Bergana, W.M. Zunic, J. Raman Spectrosc. 23 (1992) 357–363.
[53] L.E. Orgel, An Introduction to Transition-Metal Chemistry, Methuen, London, 1967.
[54] L.G. Hulett, D.A. Thornton, Spectrochim. Acta A 29 (1973) 757–763.
[55] J. Cernak, J. Kuchar, M. Stolarova, M. Kajnakova, M. Vavra, I. Potocnak, L.R. Falvello, M. Tomas, Transition Metal Chem. 35 (2010) 737–744.
[56] G.S. Kürkçüoğlu, K. Gör, O. Büyükgüngör, Spectrochim. Acta A 124 (2014) 588–594.
[57] G. Valle-Bourrouet, L.W. Pineda, L.R. Falvello, R. Lusar, T. Weyhermueller, Polyhedron 26 (2007) 4470–4478.
[58] K.B. Girma, V. Lorenz, S. Blaurock, F.T. Edelmann, Inorg. Chim. Acta 359 (2006) 364–368.
[59] B. Morzyk-Ociepa, E. Rózycka-Sokołowska, D. Michalska, J. Mol. Struct. 1028 (2012) 49–56.
[60] G. Ondrejovič, A. Kotočová, Chem. Pap. 60 (2006) 10–21.
[61] R. Hoffmann, P.V.R. Schleyer, H.F. Schaefer, Angew. Chem. Int. Ed. 47 (2008) 7164–7167.

Supplemantary material

Table 3. Atomic coordinates and thermal parameters ($Å^2$).

Atom	X	Y	Z	U_{eq}
Cu1	0.25	0.25	0.5	0.02018(7)
Cl1	0.06387(3)	0.06492(3)	0.41099(2)	0.02228(8)
N1	0.14694(9)	0.42139(11)	0.45774(8)	0.0188(2)
N4	0.33696(9)	0.34633(12)	0.35332(9)	0.0228(2)
N3	0.25973(9)	0.26925(11)	0.36706(8)	0.0180(2)
N2	0.03787(9)	0.40638(12)	0.40023(9)	0.0235(2)
C6	0.19493(11)	0.20970(15)	0.27682(10)	0.0211(3)
C5	0.23130(14)	0.24923(15)	0.20486(11)	0.0282(3)
C1	-0.01304(12)	0.53629(15)	0.37269(12)	0.0289(3)
C3	0.16542(11)	0.56453(14)	0.46628(10)	0.0228(3)
C4	0.32193(13)	0.33660(16)	0.25639(12)	0.0279(3)
C2	0.06685(12)	0.64139(15)	0.41377(12)	0.0271(3)

Table 5. Experimental and theoretical geometric parameters.

Bond Lengths(Å)	Exp.	6-311+(3df,p)	lanl2dz	Bond Angles (°)	Exp.	6-311+(3df,p)	lanl2dz
Cu1-N1	2.0033	2.048	2.041	N4-N3-Cu1	125.50	119.9	120.5
Cu1-N1	2.0033	2.048	2.041	N1-N2-C1	111.78	111.2	110.8
Cu1-N3	2.0176	2.048	2.041	N1-N2-H2N	124.10	116.6	116.2
Cu1-N3	2.0176	2.048	2.041	C1-N2-H2N	124.10	132.2	133.0
N1-C3	1.3285	1.331	1.353	N3-C6-C5	110.16	110.0	109.7
N1-N2	1.3387	1.342	1.373	N3-C6-H6	124.90	119.6	119.7
N4-C4	1.3438	1.343	1.366	C5-C6-H6	124.90	130.4	130.6
N3-N4	1.3494	1.342	1.373	C4-C5-C6	105.51	105.0	105.5
N4-H4N	0.8600	1.029	1.032	C4-C5-H5	127.20	127.4	127.1
N3-C6	1.3311	1.331	1.353	C6-C5-H5	127.20	127.6	127.4
N2-C1	1.3418	1.343	1.366	N2-C1-C2	106.99	107.2	107.2
N2-H2N	0.8600	1.029	1.032	N2-C1-H1	126.50	121.3	121.8
C6-C5	1.397	1.401	1.421	C2-C1-H1	126.50	131.5	131.0
C6-H6	0.930	1.079	1.080	N1-C3-C2	110.60	110.0	109.8
C5-C4	1.372	1.383	1.403	N1-C3-H3	124.70	119.6	119.7
C5-H5	0.930	1.077	1.079	C2-C3-H3	124.70	130.4	130.6
C1-C2	1.368	1.383	1.403	N4-C4-C5	107.05	107.2	107.2
C1-H1	0.930	1.078	1.079	N4-C4-H4	126.50	121.3	121.8
C3-C2	1.3947	1.401	1.421	C5-C4-H4	126.50	131.5	131.0
C3-H3	0.930	1.079	1.080	C1-C2-C3	105.07	105.0	105.5
C4-H4	0.930	1.078	1.079	C1-C2-H2	127.50	127.4	127.2
C2-H2	0.930	1.077	1.079	C3-C2-H2	127.50	127.6	127.4
Cu1-Cl1	2.8226	2.856	2.847				

Bond Angles (°)				Torsion Angles(°)			
N1-Cu1-N1^{i}	180.00	180.0	180.0	C4-N4-N3-C6	0.09	0.1	0.1
N1-Cu1-N3	88.40	89.7	89.7	C4-N4-N3-Cu1	179.33	179.1	179.0
N1^{i}-Cu1-N3	91.60	89.7	89.7	C3-N1-N2-C1	-0.32	0.1	0.0
N1-Cu1-N3^{i}	91.60	89.7	89.7	Cu1-N1-N2-C1	-173.60	-179.1	-179.0
N1^{i}-Cu1-N3^{i}	88.40	89.7	89.7	N4-N3-C6-C5	0.02	0.0	-0.1
N3-Cu1-N3^{i}	180.00	180.0	180.0	Cu1-N3-C6-C5	-179.19	-178.9	-178.9
C3-N1-N2	105.56	106.6	106.7	N3-C6-C5-C4	-0.11	0.0	-0.1
C3-N1-Cu1	131.81	133.5	132.8	N1-N2-C1-C2	0.36	-0.1	0.0
N2-N1-Cu1	122.19	119.9	120.5	N2-N1-C3-C2	0.15	0.0	0.0
C4-N4-N3	111.32	111.2	110.8	Cu1-N1-C3-C2	172.52	178.9	178.9
C4-N4-H4N	124.30	132.2	133.0	N3-N4-C4-C5	-0.16	-0.1	0.0
N3-N4-H4N	124.30	116.6	116.2	C6-C5-C4-N4	0.16	0.1	0.0
C4-N3-N4N	106.00	106.6	106.7	N2-C1-C2-C3	-0.24	0.0	0.0
C6-N3-Cu1	128.53	133.5	132.8	N1-C3-C2-C1	0.06	0.0	0.0

Symmetry codes : (i) (-x+½, -y+½, -z+1)

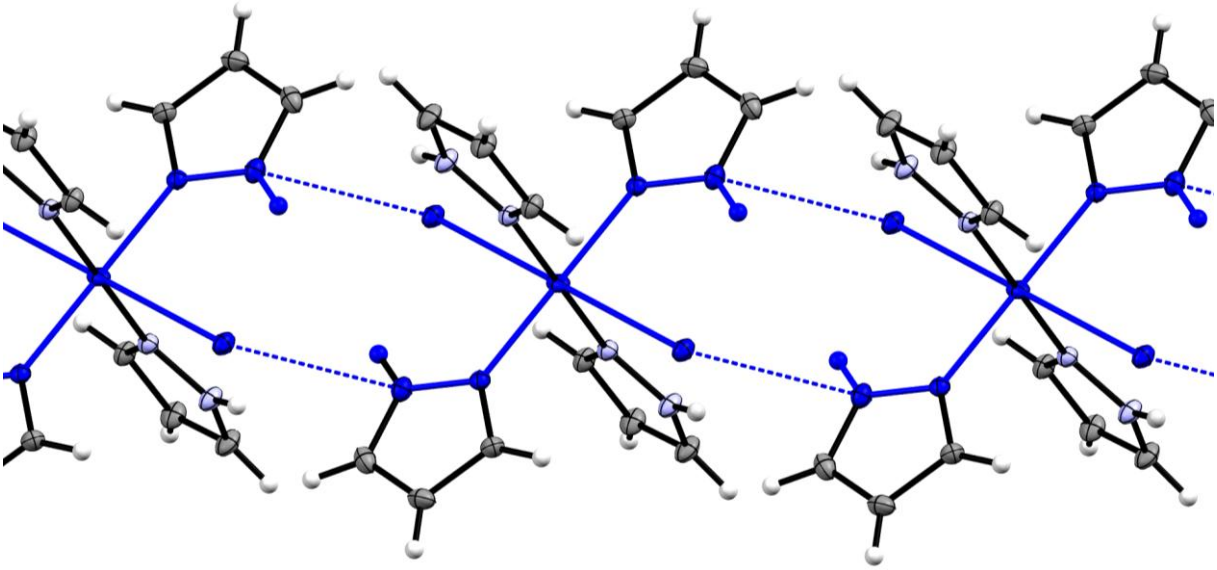

(c)

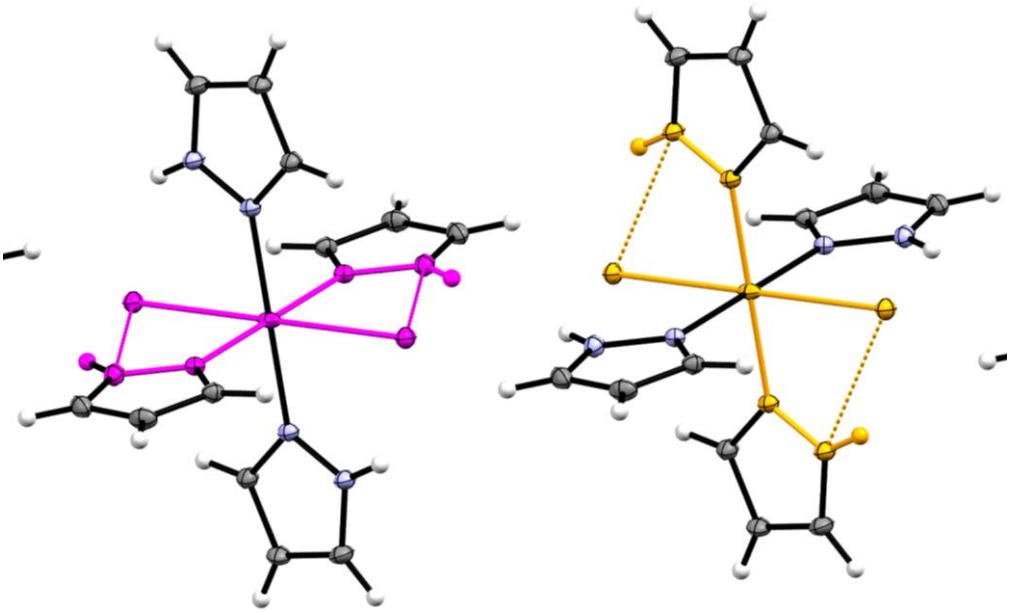

(d)

Figure 3. (c) The C(5) and $R^2_2(10)$ first-level graph set descriptors within the title compound highlighted in blue. (d) A crystal structure fragment dispalying the [$D^2_2(9)$, R(5)] and [$D^2_2(7)$ and R(5)] graph sets drawn in orange and purple, respectively.